Journal of Materials Chemistry A

Accepted Manuscript

ROYAL SOCIETY OF CHEMISTRY

www.rsc.org/materialsA

Highly stable CuS and CuS-Pt catalyzed Cu_2O/CuO heterostructure as efficient photocathode for hydrogen evolution reaction

Amare Aregahegn Dubale[1], Andebet Gedamu Tamirat[1], Hung-Ming Chen[1], Taame Abraha Berhe[2], Wei-Nien Su[2,*] and Bing-Joe Hwang[1,3*]

[1] NanoElectrochemistry Laboratory, Department of Chemical Engineering, National Taiwan University of Science and Technology, Taipei 106, Taiwan.

[2] NanoElectrochemistry Laboratory, Graduate Institute of Applied Science and Technology, National Taiwan University of Science and Technology, Taipei 106, Taiwan.

[3] National Synchrotron Radiation Research Center, Hsinchu 30076, Taiwan.

* Corresponding authors: bjh@mail.ntust.edu.tw

Abstract:

A Cu_2O/CuO heterostructure modified with CuS is proposed as a highly promising and stable photocathode for solar hydrogen production. The Cu_2O/CuO/CuS heterostructure were synthesized by in situ growth of Cu_2O/CuO via simple eletrodeposition of Cu film followed by annealing in air, and then the surfaces of the heterostructure are sequentially modified by loading CuS via successive ion Layer adsorption and reaction (SILAR) approach. Experimental evidences, including Raman, XANES/EXFS and XPS, are presented for the interfacial reaction between CuS and Cu_2O/CuO. The optimized Cu_2O/CuO/CuS photocathode provided remarkably enhanced photocurrent density of – 5.4 mA /cm^2 (i.e. > 2.5 times than that of the bare Cu_2O/CuO) at 0 V vs. RHE under standard AM 1.5 light illumination. Due to the bicatalytic effects in suppressing the electron- hole recombination, a further increase in photocurrent density, – 5.7 mA/cm^2 was noticed after decorating the Cu_2O/CuO surface with both CuS and Pt. To the best of our knowledge, this is the highest performance yet reported for a cocatalyst modified Cu_2O/CuO photoelectrode for solar water splitting. More importantly, the Cu_2O/CuO heterostructure modified with optimum CuS afforded an impressive solar conversion efficiency of ABPE% = 3.6% which is greater than fourfold increase compared with the bare Cu_2O/CuO. The stability of the bare Cu_2O/CuO photocathode showed about a 44% decrease in initial photocurrent density within 1 h, whereas 85% and 92% of the initial photocurrent is maintained after 1 h when the photocathode was modified with CuS and with both CuS and Pt respectively. This highly

enhance photoectrochemical property is attributed to the fast transfer of photogenerated electrons resulting in suppressed electron-hole recombination and synergistic effects of heterojunction in light absorption and charge separation. The work demonstrates a facile strategy and potential use of low cost CuS as efficient cocatalyst for solar hydrogen production that can be applicable in the general field of energy conversion.

Keywords: Photoelectrochemical water splitting; Cu_2O/CuO; heterostructure; CuS; cocatalyst; photocathode; hydrogen production

1. Introduction

The conventional fossil resources such as natural gas, coal and petroleum are common energy demand used by the society for powering vehicles or electric devices. However, due to their cost, global warming effect and logically forecasted to be exhausted in the future, replacement of fossil fuels by renewable energy resources is highly inescapable. Hydrogen is regarded as a next-generation energy carrier if it is produced from renewable energy sources.[1] Hydrogen evolution via photoelectrochemical (PEC) water splitting is one possible and attractive means of hydrogen generation because it requires only semiconductor electrodes, water, and sunlight.[2]

The hydrogen generation performance of the semiconductor materials depends on their optical and electronic properties. To harvest maximum visible light, the semiconductors should have appropriate band gap for sunlight absorption, suitable band positions for water reduction/oxidation, and stability under the required reaction conditions.[1, 3] It is reported that many semiconductors, such as TiO_2, $SrTiO_3$, WO_3, CdS and so on,[4-9] have shown the ability to generate hydrogen. Compared to them, Cu_2O with a relatively narrow band gap (ca. 2.0 eV), makes it effective in harvesting visible light[10, 11] and sufficiently more negative conduction band edge, is more promising and attractive material for solar driven hydrogen production. The maximum absorption of visible light by its band gap will provide a theoretical photocurrent of 14.7 $mAcm^{-2}$ and a light-to-hydrogen conversion efficiency of 18% based on the AM 1.5 spectrum.[12] Furthermore, copper is inexpensive and naturally abundant and thus offers the potential for cost-competitive large-scale Cu_2O photoelectrode fabrication.[13] However, poor photostability in aqueous electrolytes combined with low photocatalytic efficiency caused by fast recombination of minority carriers still severely limits the practical utilization of Cu_2O in solar hydrogen production. Recently, researchers have investigated the possibility of using protective layers[14-16] to enhance the stability and PEC performance of the Cu_2O based photoelectrodes. In fact, in literatures, it seems challenging to achieve photoelectrodes that exhibit enhanced stability and PEC performance at the same time. For instance, although –7.6 mA/cm^2 at 0 V vs. RHE is the activity of the world record achieved with Cu_2O photocathode protected with layer by layer deposited inorganic oxides and overcoated with Pt cocatalysts,[14] the stability of the photocathode is still quite low (i.e. 67% of the initiation photocurrent density was decayed after 20 minutes of

illumination). Of course, coupling Cu_2O with other semiconductors, such as CuO [2, 17, 18], TiO_2 WO_3[19] and $BiVO_4$[20] with appropriate band alignments can provide an interface for the charge transfer, and then improve the photoactivity for H_2 production. However, without appropriate surface modification by cocatalysts, for instance with Pt[14], RuO_2[21], MoS_2[22, 23] and so on, the Cu_2O either protected with protective layers alone or coupled with semiconductors cannot give high hydrogen evolution activities, which is because of the fast recombination of photogenerated electron-hole pairs before migrating to the surface for reactions. Thus, the presence of cocatalyst not only effectively separates the electron-hole pairs but also provides more proton reduction sites, facilitating proton reduction reactions.[24]

Even though the noble metals and transition metal oxides or sulfides could be the efficient cocatalyts for PEC water splitting, their high cost and availability highly limits their utilization in real application. Therefore, it is very important to develop highly efficient and low-cost noble-metal free cocatalysts to further facilitate the development of hydrogen evolution. In our recent work, it was found that CuO can act as an excellent component for fabricating heterostructure with Cu_2O, and the PEC activity of Cu_2O/CuO for H_2 evolution was greatly enhanced by loading nickel nanoparticles as a cocatalyst on Cu_2O/CuO.[2] It is also reported that WS_2 and MoS_2 play a vital role as cocatalyst on semiconductors such as CdS[25] or Cu_2O[13] and hydrogen evolution was greatly enhanced. However, tungsten and molybdenum are also rare metals. Copper sulfide (CuS), which is an important photoelectric material with superior performance, is earth-abundant and has drawn intense attention owing to its application in lithium ion batteries, photocatalysts, solar cells and gas sensors.[26-29] Therefore, research into CuS as a cocatalyst for photocatalytic hydrogen evolution from water splitting has extremely vital significance. Recently, independent studies by Shen et al. and Zhang et al found that a small amount of CuS can improve the visible photocatalytic activity of $ZnIn_2S_4$ and $Zn_{0.8}Cd_{0.2}S$ respectively.[30, 31] We expect CuS could also acts as a cocatalyst on Cu_2O/CuO heterostructure if optimum amount is deposited, and to the best of our knowledge the role of loaded CuS and transfer of photogenerated charge carriers on the PEC activity of Cu_2O/CuO heterostructure have not been reported before.

Herein, for the first time we demonstrate the photoelectrochemical generation of H_2 using a Cu_2O/CuO heterostructure photocathode modified with an earth abundant and low cost CuS as

cocatalyst (Cu_2O/CuO/CuS), and with both CuS and Pt (Cu_2O/CuO/CuS/Pt). We synthesized the Cu_2O/CuO heterojunction following our previous report.[2] A facile successive ionic layer adsorption and reaction (SILAR) method using $Cu(NO_3)_2$ and Na_2S as precursors was used to deposit CuS nanoparticles on the Cu_2O/CuO heterostructure, while Pt loading is performed by sputtering procedure. At the optimized condition, the Cu_2O/CuO heterostructure modified with CuS and with both CuS and Pt provides a photocurrent density up to −5.4 mA/cm^2 and −5.7 mA/cm^2 respectively along with remarkably enhanced photostability over 1 h. In addition to detailed PEC performance measurements, a thorough pre and post characterization of the modified heterostructured photocathode was investigated with respect to its stability. We believe the method and results shown here point out a convenient and applicable approach for further exploitation of unstable materials for photoelectrochemical hydrogen production.

2. Experimental section

2.1 Methods

2.1.1 Synthesis of Cu_2O/CuO

All chemicals used in this study were of analytical grade and used without further purification. The Cu_2O/CuO heterostructure was fabricated on fluorine-doped tin oxide glasses (FTO) in two step reaction following our previous report.[2] Firstly, pair of FTO substrates, connected to DC power supply, were immersed into saturated copper ion solution prepared by dissolving $CuSO_4.5H_2O$ with deionized water. Cu films were deposited from this solution with a potential of 5 V for 2 minutes. Subsequently, the Cu_2O/CuO heterojunction was obtained *in situ* by annealing the as prepared Cu film in a cubic furnace in air at temperatures of 450 ˚C for 4 hour.

2.1.2 Deposition of cocatalyst

To enhance the kinetics of water reduction reaction stepwise deposition of CuS and Pt cocatalyst were carried out. The CuS nanoparticle was deposited on the surface of the Cu_2O/CuO using SILAR method. The Cu_2O/CuO photoelectrode was immersed into a 5 mM $Cu(NO_3)_2$ ethanol solution and subsequently into a 5 mM Na_2S ethanol solution at room temperature and for about 20 s each. Following each immersion, the photoelectrode was rinsed using pure ethanol to

remove loosely adsorbed ions from the precursor. The desired amount of CuS is controlled by repeating the immersion cycle (the number of SILAR cycle) from 3 to 15 complete cycles. For simplicity, the photoelectrode is named as Cu_2O/CuO/CuS-x, where x refers the number of CuS SILAR cycles. The deposition of Pt nanoparticles on Cu_2O/CuO/CuS photocathode was done using sputtering technique for 5 to 40 seconds.

2.2 Structure characterization

The photoelectrodes were characterized by XRD, SEM, DRS UV-Vis, Raman, XPS and XANES/EXAFS. X-ray diffraction (XRD) pattern were acquired with a D2 phaser XRD-300 W, with measurements taken using Cu K_α radiation at 40 kV and 100 mA. Spectra were obtained with a linear silicon strip `Lynx Eye' detector from 20˚ to 80˚ at a scan rate of 3˚ min^{-1}. The morphology of the electrodes were characterized using Field Emission Scanning electron microscopy (EDX JSM 6500F, JEOL) The diffuse reflectance UV-vis adsorption spectra were obtained using a JASCO (ISV-469) V 560 UV-Vis spectrometer with fine $BaSO_4$ powder as reference. Raman measurements were performed on a proMaker confocal Raman microscope system as integrated by Protrustech Co., Ltd. A solid state laser operating at λ= 532 nm was used as the excitation source with a laser power of 20 mW to circumvent degradation with 10 s exposure times and 15 accumulations. X-ray photoelectron spectroscopies (XPS) were performed at Wide-Range beamline (BL24A) of NSRRC. The UHV end station of BL24A housed a load-lock sample transfer mechanism, a differentially pumped sputter-ion gun for sample cleaning, and a SPEC Phoibos 150 energy analyzer for XPS. XPS binding energy scale was referenced to the bulk Au $4f_{7/2}$ core level located at 84.00 eV relative to Fermi level. The hard X-ray absorption spectra (XAS) were collected at the beam line BL17C1 of National Synchrotron Radiation Research Center (NSRRC) in Hsinchu, Taiwan. The storage ring of the electronic accelerator can supply the electronic energy of 1.5 GeV and the operation current at 360 mA. A Si double crystal monochromator was used to perform energy scan, of which the parallelism can be adjusted to eliminate the high order harmonics. All XAS data were recorded using the fluorescence mode.

2.3 Photoelectrochemical measurement

The photoelectrochemical performance of the electrodes was assessed in a three electrode system using an aqueous solution of 1M Na_2SO_4 buffered at pH 5 with potassium phosphate (0.1 M). The three-electrode configuration consists of Ag/AgCl in saturated KCl as reference electrode, a Pt wire as the counter electrode and the prepared Cu_2O/CuO or Cu_2O/CuO/CuS as working electrode. The photoresponse of the synthesized electrode was acquired under chopped illumination from a 300 W Xenon lamp equipped with AM 1.5 filter. The intensity of light source was calibrated with a Si diode (Newport) to simulate AM 1.5 illumination (100 mW/cm^2). For all the samples, a scan rate of 10 mV/s was used for the current versus potential measurements (LSV). Photocurrent stability tests were performed by measuring the photocurrent produced under chopped light irradiation (on/off cycles of 10 s) at a fixed biasing potential of 0 V vs. RHE. During the PEC tests, the electrolyte was constantly purged with N_2 for 30 minutes. The electrochemical impedance spectroscopy (EIS) was performed using an electrochemical impedance analyser with an AC amplitude of 10 mV and frequency range between 100 kHz to 0.1 Hz. The measured EIS data were obtained at an applied bias of 0 V vs. RHE at 25 ˚C.

2.4 Photoelectrocatalytic hydrogen measurement

The photostability measurement equipped with hydrogen quantification experiment on bare Cu_2O/CuO and Cu_2O/CuO/CuS was carried out at an applied potential of 0 V vs. RHE under AM 1.5 irradiation. The evolved gas during the reaction was collected above the water through a tube connected to a separate burette equipped with septum as head cap. The change in volume of water displaced by the generated gas was taken as total volume of evolved gas. The evolved gas sample was taken from head cap of the burette with a gas-tight syringe and analyzed using a YANGI–LiN gas chromatograph equipped with PDHID detector. Generated H_2 was carried out following the GC calibration curve made with known concentration of H_2 (5% H_2/Ar).

3. Results and discussion

3.1 Cocatalyst deposition on the photoelectrode

Copper sulfide nanoparticles on Cu_2O/CuO were loaded by successive ion layer adsorption and reaction (SILAR) of Cu_2O/CuO photoelectrodes in 5 mM ethanolic solution of copper nitrate and

sodium sulfide in each. Scheme 1 shows experimental set-up of manually operated SILAR deposition system. That is, the Cu_2O/CuO photoelectrodes fabricated by electrodeposition of Cu film (at 5 V for 2 min) on FTO followed by thermal oxidation in air (at 450 ˚C for 4 h) was firstly dipped in the cationic precursor solution ($Cu(NO_3)_2$) for 20 s, resulting Cu^{2+} to be adsorbed onto the surface of Cu_2O/CuO films (Scheme 1a). Subsequently, this photoelectrode was immersed in ethanol solution for 30 s to remove excess adsorbed ions from the precursor (Scheme 1b). Thirdly, the sample was then immersed in the anionic precursor solution (Na_2S) for 20 s, resulting reaction of sulfide ion (S^{2-}) with the adsorbed Cu^{2+} on the surface of Cu_2O/CuO photoelectrode (Scheme 1c). In the final step of the SILAR process, the excess and/or unreacted species and the reaction byproduct from the diffusion layer are removed by rinsing the photoelectrode in pure ethanolic solution (Scheme 1e). Therefore, one cycle of CuS deposition on the surface of Cu_2O/CuO photoelectrode was accomplished. The built-in amount of CuS can be increased by repeating the immersion cycles. The ionic reaction that could takes place during the SILAR process is given as follows:

$$Cu^{2+} + S^{2-} \longrightarrow CuS \qquad (1)$$

Finally, the Cu_2O/CuO/CuS-Pt structure was obtained via sputtering of Pt for desired time of deposition.

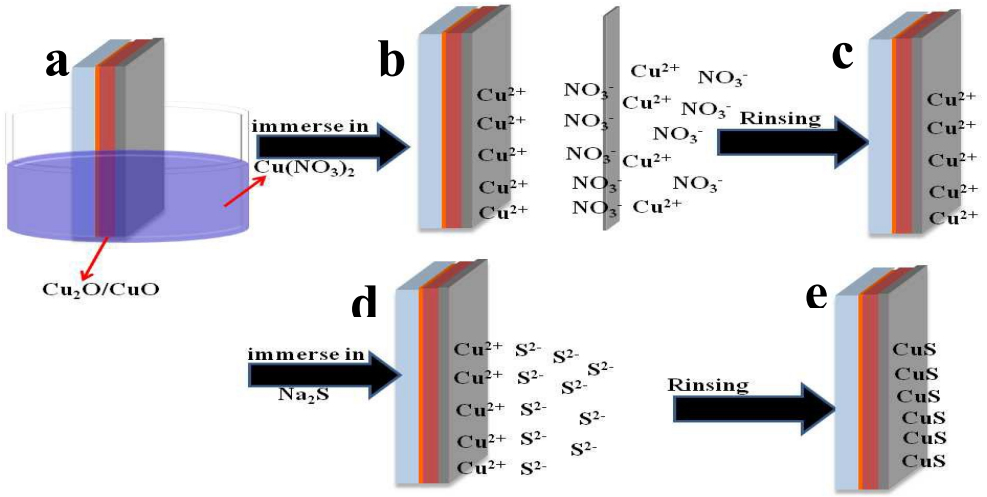

Scheme 1. Illustration of SILAR growth: (a) Immersion of Cu_2O/CuO in $Cu(NO_3)_2$ solution (b) Adsorption of $Cu^{2+}NO_3^-$ and the formation of electrical double layer, (c) rinsing (I) removes excess, unabsorbed Cu^{2+} and NO_3^-, (d) reaction of S^{2-} with pre-adsorbed Cu^{2+} ions to form CuS

and (e) rinsing (II) to remove excess and unreacted species and form the solid solution CuS on surface of the substrate.

3.2 Photoelectrode Characterizations with XRD, Raman and SEM

The typical XRD patterns of the bare Cu_2O/CuO and the Cu_2O/CuO modified with CuS are shown in Figure 1(a). In all the samples, the emerged XRD diffraction peaks at 36.4 and 38.9˚ could be indexed to the (111) crystal planes of Cu_2O (JCPDS card number 05-0667) and CuO (JCPDS card number 5-661) respectively. This implies that well crystallized cubic Cu_2O and monoclinic CuO nanostructures are found in the XRD patterns.[2] It is noted that no characteristic diffraction peaks for CuS can be observed in any of the Cu_2O/CuO modified with CuS samples for 3 to 15 SILAR deposition cycles. This is because of the low content of CuS loading. To confront this issue, we also measured XRD pattern of the Cu_2O/CuO modified with CuS for many SILAR deposition cycles, revealing a small emerging peaks at 48.8˚ which corresponds to the (110) planes of crystalline CuS (JCPDS file No. 65-3931). This indicates the formation of Cu_2O/CuO/CuS nanostructure by the SILAR process.

The loading of CuS on the surface of Cu_2O/CuO under our SILAR procedure was analyzed and a good quality Raman spectra were obtained as shown in Figure 1b. In the Raman spectra of the bare Cu_2O/CuO and the Cu_2O/CuO modified with three SILAR cycles (Figure 1b), the weak peak at 218 cm^{-1} and relatively strong peak at 286 cm^{-1} can be assigned to the Cu_2O and CuO component of the heterostructure. Upon increasing the SILAR deposition cycle from 3 to 15, it is hardly to observe the characteristic peaks of Cu_2O (218 cm^{-1}), indicating the SILAR process increases the CuS film growth on the surface of the heterostructure and limits the detection of Cu_2O components in the bulk. For the Cu_2O/CuO photoelectrodes modified with 3 to 15 deposition cycles, the newly emerged peak at 470 cm^{-1} attributed to the S–S bonds vibrational (stretching) modes, confirming the formation of hexagonal CuS, also by correlation with the XRD results. The shift to a lower Raman shift values (compared to the reference 474 cm^{-1},[32]) may be associated with the vacancies in the CuS lattice, induced during the film growth.[33]

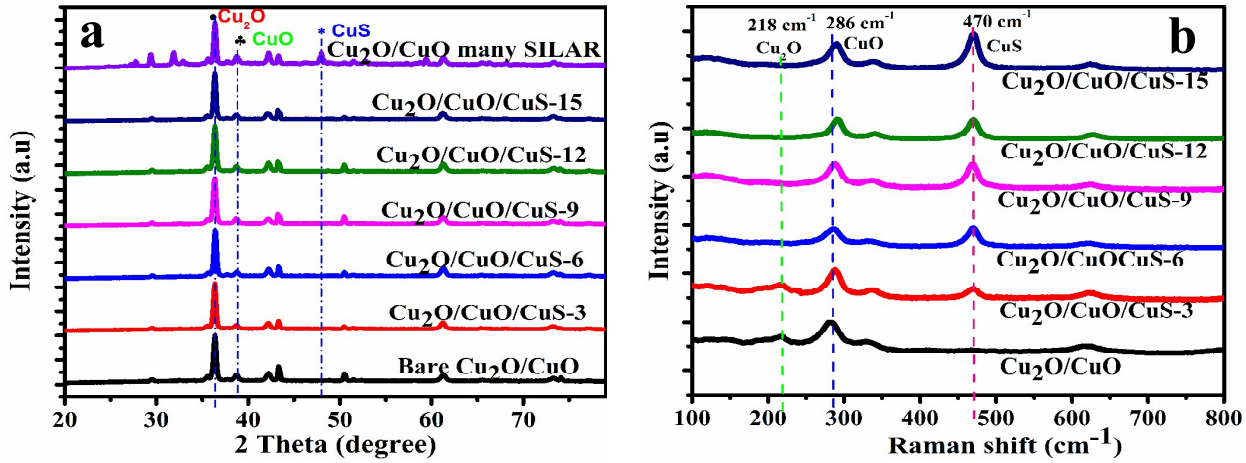

Figure 1. (a) XRD patterns and (b) Raman spectra of bare Cu_2O/CuO and 3, 6, 9, 12 and 15 times SILAR of CuS on Cu_2O/CuO.

To observe the possible deposition of CuS nanoparticles on the surface of Cu_2O/CuO at different SILAR deposition cycle, we carried out scanning electron microscope (SEM) measurements both before and after CuS deposition at various cycle, shown in Figure 2 and S1. It is shown in Figure 2a that the as prepared Cu_2O/CuO exhibit highly dense and uniform film features. Once the modification of CuS nanoparticles was carried out for three SILAR cycle on the surfaces of Cu_2O/CuO, a few nanoparticles appeared on the surface of Cu_2O/CuO. These are clearly indicated by small circles in the SEM image (Figure S1a). As the SILAR deposition cycles increased from 3 to 15 (Figure 2 and S1), the amount of the CuS particles deposited on the surface of the heterostructure increased rapidly. This implies that the CuS nanoparticles indeed deposited onto the surfaces of the Cu_2O/CuO by the SILAR method. The energy-dispersive X-ray (EDX) spectrum (Figure S2) also confirms that the Cu_2O/CuO/CuS sample consists of copper, oxygen and sulfur elements. The presence of Pt in addition to copper, oxygen and sulfur elements in the EDX spectrum of Cu_2O/CuO/CuS/Pt sample confirms the deposition of platinum (Figure S2b).

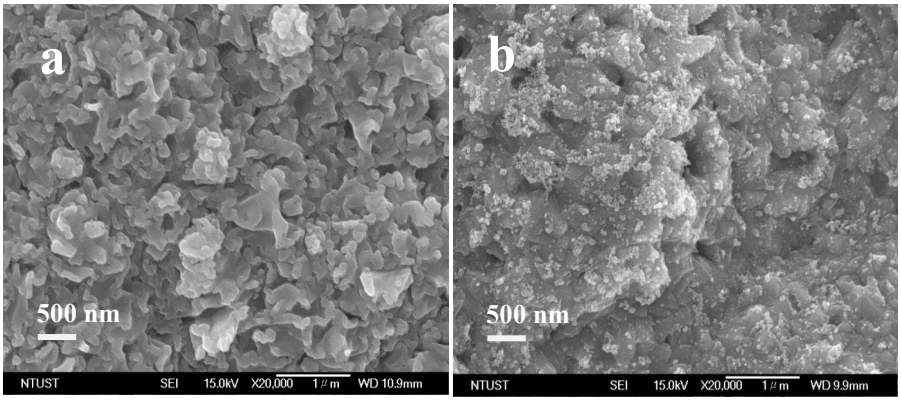

Figure 2. Scanning electron microscopy images of Cu_2O/CuO (a) and Cu_2O/CuO/CuS-9 (b)

3.3 Photoelectrochemical Characterization

To investigate the PEC performance of the bare Cu_2O/CuO, CuS loaded Cu_2O/CuO at various SILAR cycle (Cu_2O/CuO/CuS-x) and both CuS and Pt loaded Cu_2O/CuO photocathodes, linear sweep voltammetry measurements were performed in 1 M Na_2SO_4 electrolyte (pH) 5) under chopped AM 1.5G (100 mW cm^{-2}) illumination using a conventional three electrode system, with the Cu_2O/CuO/CuS-x photocathode, Ag/AgCl electrode and Pt wire as working electrode, reference electrode, and counter electrode, respectively. A Cu_2O/CuO electrode without CuS loading generated a photocurrent density of 2.2 mA cm^{-2} at 0 V vs RHE (Figure S3a1) which is consistent with our earlier report. Compared with the PEC activity of the Cu_2O/CuO photoelectrods modified with CuS or with both CuS and Pt (that will be discussed in this section), this value is much lower. The lower photocurrent density was attributed to the sluggish kinetics and self reduction of the CuO protective layers. However, after deposition of optimum CuS nanoparticles i.e. for nine SILAR cycles on the Cu_2O/CuO heterostructure, a significantly improved photocurrent density as high as –5.4 mA/cm^{-2} was achieved at water reduction potential (0 V vs. RHE, Figure 3(a1)). This value is more than 2.5 higher than the photocurrent density of the unmodified Cu_2O/CuO photoelectrode (–2.2 mA/cm^2, Figure S3a1). The enhanced performance is primarily due to the worthy catalytic activity of CuS that facilitates a rapid electron transfer to the electrolyte so as to suppress recombination at the surface. Therefore, the cycle of SILAR deposition of CuS was optimized as 9 cycle in the present study. The relatively

low photocurrent density at lower SILAR cycles (3 and 6 cycles) is likely due to the CuS deficiency increases electron-hole recombination.

The PEC performances of all Cu_2O/CuO/CuS-x photoelectrodes are presented in Figure S3 and summarized in Figure 4. The photocurrent density of the photoelectrodes increases with increasing the SILAR cycles and reached a maximum value (–5.4 mA/cm^2) at the CuS deposition for nine SILAR cycle. However, the fading PEC performance on the Cu_2O/CuO/CuS-x photoelectrodes was detected when the SILAR deposition cycle increases from 9 to 15 likely due to several possible reasons. This is presumably first because of excessive CuS formed on the surface of Cu_2O/CuO may block the incoming light to the heterostructure material and thus reduces electron generation. Secondly, the increase of their particle size results in worsening of the catalytic activity of CuS clusters or disappearance of surface effect. Thirdly, CuS at high content may act as charge recombination centers, resulting in the decrease of the photocatalytic activity. It is also observed that the photocurrent onset potential of the optimized photocathode (Cu_2O/CuO/CuS-9) shifted to the more positive value (~0.62 V vs. RHE) than the bare Cu_2O/CuO (~0.54 V vs. RHE). The noted shift in onset potential can be attributed to the presence of CuS cocatalyst. This is advantageous in lessening the voltage requirement from the photoanodes and significantly improves the water splitting efficiency.

To further enhance the PEC performance of the photoelectrode and to investigate the effect of dual cocatalyst, we carried out Pt deposition on top of the optimized electrode (Cu_2O/CuO/CuS-9) using sputtering technique. Pt sputtering on the surface of Cu_2O/CuO/CuS-9 electrode was carried out for 5, 10, 15, 20 and 40 seconds. As shown in Figure 3(b1), under chopped illumination, the Cu_2O/CuO/CuS nanostructure sputtered with Pt for 10 second (Cu_2O/CuO/CuS/Pt, the rest results are not shown here) provided the maximum photocurrent density, –5.7 mA/cm^2 at 0 V vs. RHE, i.e. more than 2.6 and 1.1 times higher than the photocurrent density of the Cu_2O/CuO and Cu_2O/CuO/CuS photoelectrode respectively. This indicates that CuS and Pt could also be used as a cocatalyst that provides high PEC performance for hydrogen evolution due to their dual function in facilitating the charge transport and suppression of the possible electron-hole recombination. The photocurrent density achieved in this study is highly competitive with the highest values reported in literature.

To examine the stability of the photoelectrodes, the time course of the photocurrent density was measured at 0 V vs. RHE in chopped AM 1.5 light illumination. The photocurrent density of as-prepared Cu_2O/CuO heterostructure decreases to about 56% of the initial photocurrent density within 1 h (Figure 4 and S3a2). The decrease of the photocurrent probably results from the surface degradation by continuous surface charging during illumination. After optimum CuS deposition, the photocurrent density is quite stable and 85% of the initial photocurrent is maintained after 1 h (Figure 3a2), indicating that CuS has cocatalytic activity on H_2 evolution because of its redox potential (CuS/Cu_2S) is more negative than the H^+/H_2. The higher photostability of CuS modified heterostructure (Cu_2O/CuO/CuO-9) is also attributed to fast transfer of photogenerated electrons and suppressed electron-hole recombination due to the interfacial charge transfer (IFCT) initiated by visible light illumination (evidenced by XPS in later section). Figure 4 and S3 presents the comparison of photostability as a function of CuS deposition cycle and the photocurrent density- time curves for the Cu_2O/CuO/CuS-x photoelectrodes respectively.

The photostability measurements done on Cu_2O/CuO modified with both CuS and Pt shows significantly stable photocurrent current density i.e. 92% of the initial photocurrent is maintained after 1 h (Figure 3b2), indicating that dual catalytic effect further enhances the charge transfer and stability of the photoelectrode. As shown in Figure 4 and Figure S3, all Cu_2O/CuO/CuS-x photocathodes showed significantly improved photostability, increasing almost linearly with increase in SILAR deposition of CuS before reaching a highland at 85% with nine cycle of CuS deposition (Cu_2O/CuO/CuO-9).

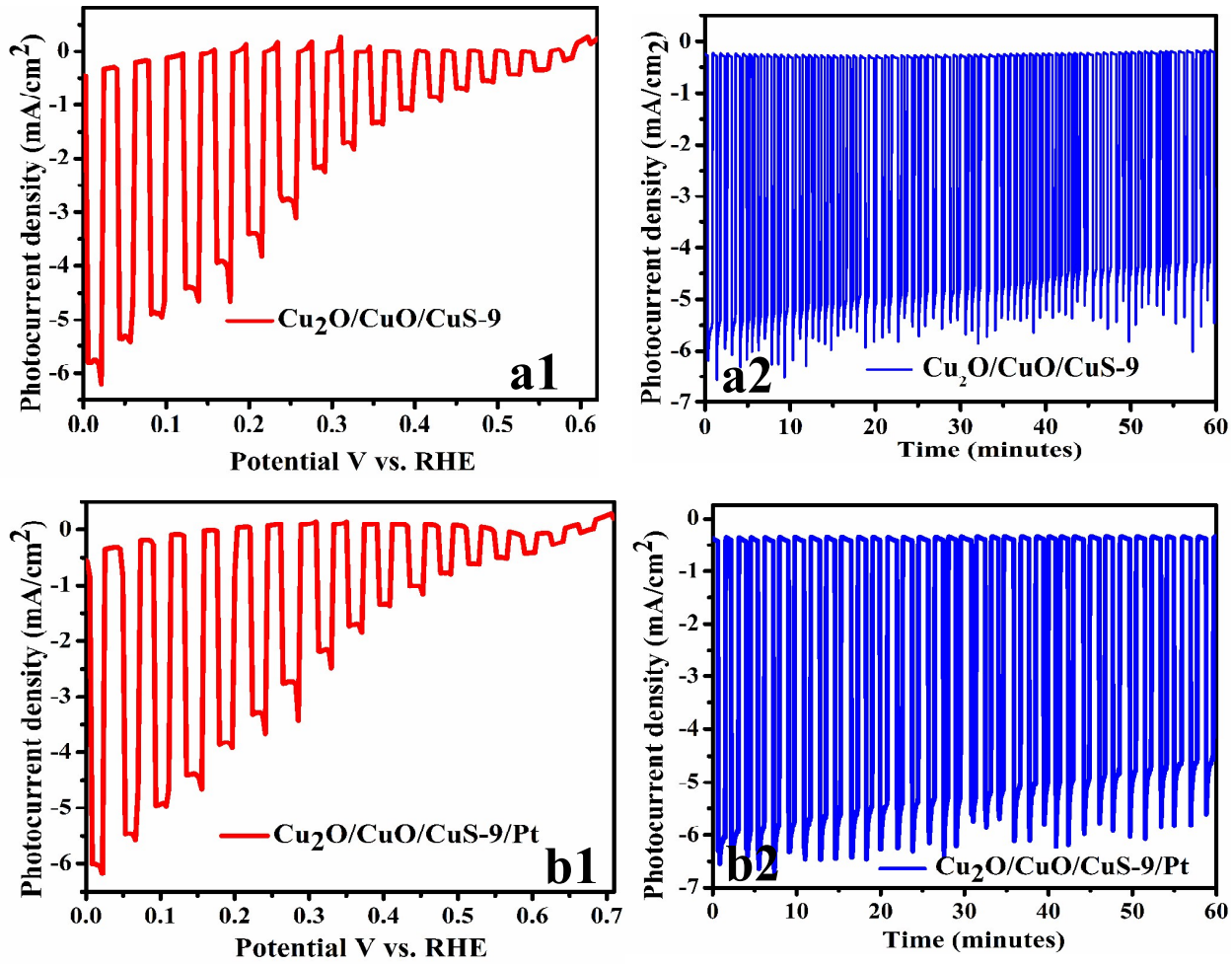

Figure 3. PEC performances and stability measurement of Cu_2O/CuO/CuS-9 (a1 and a2), and Cu_2O/CuO/CuS-9/Pt (b1 and b2).

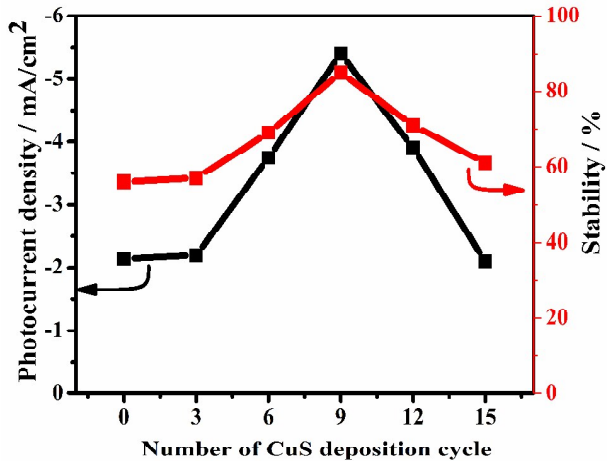

Figure 4. Photocurrent density and photostability (measured at 0 V vs. RHE) of the Cu_2O/CuO/CuS-x photocathodes as a function of number of CuS deposition cycle.

During the photostability measurements a substantial generation of bubble accompanied with appreciable cathodic photocurrent density was unequivocally observed on the electrode surface, indicating the evolution of hydrogen gas. To further confirm the generated cathodic photocurrent density is associated with hydrogen evolution, we carefully carried out quantification of evolved H_2 during the hydrogen experiment using gas chromatography within 20 minutes. After passing 2.8 C (Figure 5a, obtained from integrating the measured current over time) through the Cu_2O/CuO/CuS-9 photocathode at 0 V vs. RHE under AM 1.5 illumination, 0.0126 mmole H_2 was detected (Figure 5b), giving a faradic efficiency of 87%. At the same conditions, the bare Cu_2O/CuO photocathode evolved less than 3.5 times less H_2, i.e. 0.0035 mmole, after passing 1.2 C, corresponding to a faradaic efficiency of 56%. Compared with bare Cu_2O/CuO, a 1.5 fold increase in faradaic efficiency with Cu_2O/CuO/CuS-9 indicates the valuable effects of CuS modification for H_2 production. That is, a much more efficient H_2 production achieved with Cu_2O/CuO/CuS-9 photocathode could be presumably due to the active sites provided by the CuS nanoparticles on the surface of Cu_2O/CuO and also the good interaction between the materials. The far deviation in faradaic efficiency from unity with Cu_2O/CuO was due to the degradation of the photoelectrode itself whereby the photogenerated electrons are not effectively utilized for hydrogen evolution: this is evidenced by SEM, XPS and XANES studies in the following section and in the SI. However, the slight deviation in faradaic efficiency from unity with CuS modified

Cu_2O/CuO (Cu_2O/CuO/CuS-9) photoelectrode was not evidenced due to degradation of the photoelectrode itself, rather presumably due to unwanted backward reactions between H_2 and O_2,[34] or dissolution in the electrolyte solution.[35] In spite of these limitations, the current study demonstrates that the Cu_2O/CuO photocathode modified with CuS has a better PEC performance with suppression of photocorrosion property compared to the bare Cu_2O/CuO photocathode.

The solar conversion efficiency of PEC water splitting was also evaluated by computing the applied bias photon-to-current efficiency (ABPE) in a two electrode system according to the following equation:[36]

$$\mathrm{ABPE} = \left[\frac{|j_{ph}|(\mathrm{mA/cm^2}) \times (1.23 - |V_b|)(\mathrm{V})}{P_{total}(\mathrm{mW/cm^2})}\right]_{\mathrm{AM\ 1.5G}}, \quad (2)$$

where j_{ph} is the photocurrent density obtained under an applied bias V_b between the working and the counter electrodes, 1.23 V is the standard water splitting reaction potential and P_{total} is the incident light intensity (which is 100 mW/cm^2). As shown in Figure 5c, the maximum solar conversion efficiency (ABPE%) for the Cu_2O/CuO/CuS reaches approximately 3.6% at an applied bias of −0.43 V vs. the Pt counter electrode while the bare Cu_2O/CuO photoelectrode exhibits a maximum efficiency of 0.87% at the same applied bias and measuring conditions. This enhancement is probably attributed to efficient surface charge transfer and suppressed electrons-holes recombination by the CuS nanoparticles.

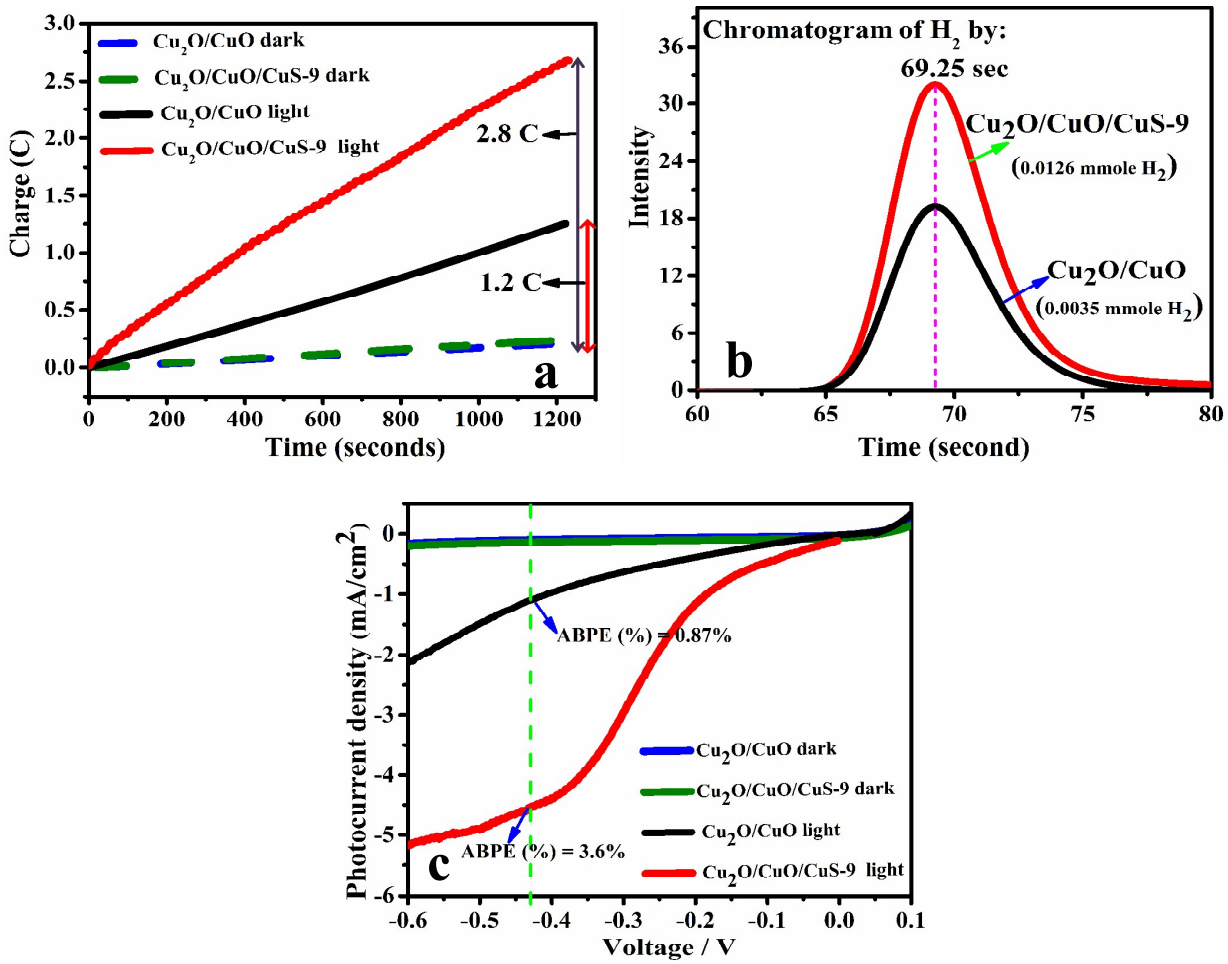

Figure 5. (a) Electrolysis response of Cu_2O/CuO and Cu_2O/CuO/CuS-9 photocathodes at an applied potential of 0 V vs. RHE under visible light illumination and dark condition (b) Chromatogram of H_2 measurement for the photostability test (c) Linear sweep voltammetry of Cu_2O/CuO and Cu_2O/CuO/CuS-9 in two electrode system (vs. Pt) under simulated one sun illumination (100 mW/cm^2).

3.4 Charge transfer studies on photocathode

In order to understand the role of CuS, electrochemical impedance spectra (EIS) measurements were carried out to investigate the photogenerated charge transfer activity at the photocathodes/electrolyte interface. The EIS of Cu_2O/CuO/CuS-9/Pt, Cu_2O/CuO/CuS-9 and bare Cu_2O/CuO photoelectrodes under simulated one sun illumination and dark conditions at a potential of 0 V vs. RHE are shown in Figure 6(a). It is known that the semicircular feature of the Nyquist plots (Figure 6(a)) at high frequencies is the defining characteristic of the charge

transfer process where the diameter of the semicircle is equal to the charge transfer resistance (R_{ct}).[37] For all the photocathodes the charge transfer resistance (R_{ct}) under light was much lower than that in the dark because of the higher charge carrier densities induced by photoexcitation. The Cu_2O/CuO/CuS-9 photocathode by far revealed a lower R_{ct} value and higher conductivity than the bare Cu_2O/CuO whilst competitive enough values with both CuS and Pt catalyzed Cu_2O/CuO (Cu_2O/CuO/CuS-9/Pt) photoelectrode both in the dark and under illumination. This indicates that incorporating CuS as a cocatalyst could better facilitate the electron transfer from the photocathode to the electrolyte, resulting better PEC performance with best stability. Similar phenomenon, i.e. the activity of CuS as a cocatalyst, was also obtained by the linear scan voltammograms recorded for Cu_2O/CuO and Cu_2O/CuO/CuS-9 in 1 M Na_2SO_4 solution under dark condition (Figure 6b). The photocurrent density versus potential curves show the generation of cathodic currents for the reduction of protons at the modified photoelectrodes. More interestingly, the potential recorded for the reduction of proton at the Cu_2O/CuO photoelectrode is –0.37 V (vs. RHE), while the proton reduction potential increased to –0.18 V (vs. RHE) for the Cu_2O/CuO/CuS photoelectrode. The considerable decrease of the overpotential of H^+ reduction for Cu_2O/CuO/CuS can be ascribed to the active site provided by the CuS nanoparticles on the surface of Cu_2O/CuO and also the good interaction between the two materials, therefore improving the electron transfer rate, facilitating holes/electrons separation at the surface, and thus enhancing kinetics of water reduction.[13]

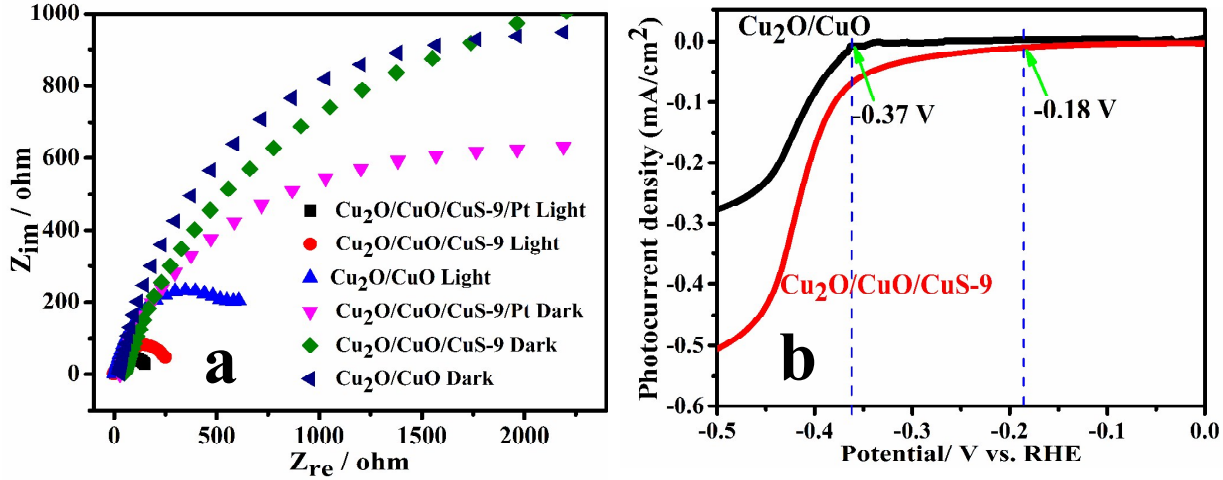

Figure 6. (a) Nyquist plots of selected photocathodes both in dark and under AM 1.5 illumination in 1.0 M Na_2SO_4 electrolyte buffered at pH 5.0 (b) linear scan voltammograms

recorded for Cu_2O/CuO and Cu_2O/CuO/CuS-9 in 1 M Na_2SO_4 solution (pH 5.0) under dark condition.

3.5 Photostability Characterization

To examine the chemical composition of the photocathodes, XANES and EXAFS were taken for Cu_2O/CuO and Cu_2O/CuO/CuS-9 samples both before and after the PEC test (see Figure 7(a)). Even though the XANES spectra of Cu_2O/CuO and Cu_2O/CuO/CuS-9 before PEC test (Figure 7a) have the similar features, the XANES spectra of Cu_2O/CuO/CuS-9 photoelectrode before PEC test is slightly shifted to the higher energy (see inset in Figure 7a), indicating that oxidation taking place during incorporation of CuS. On the other hand, after PEC test the edge position of Cu_2O/CuO is shifted 0.5 eV to a lower position, indicating the average oxidation state of Cu species is reduced: this reduction was found to be significantly suppressed after incorporating CuS. The CuS modified photocathode (Cu_2O/CuO/CuS-9) showed a relatively smaller shift in edge position (0.2 eV) after the PEC test (in the direction shown in inset in Figure 7(a)), indicating the better stability of the heterojunction probably due to the oxidation-reduction phenomenon incorporated as a result of CuS species. A significant morphological surface change (degradation) phenomenon was clearly observed after PEC test by the bare Cu_2O/CuO while the CuS modified Cu_2O/CuO (Cu_2O/CuO/CuS-9) did not show any significant change in morphology after 20 minutes of illumination (Figure S4).

In harmony with the XANES spectra, the Fourier transform magnitudes Cu-*K*- edge EXAFS spectra (shown in Figure 7(b)) of Cu_2O/CuO/CuS-9 both before and after the PEC test are similar with two main peaks below 3.5 Å. The first peak located at about 1.6 Å is due to the Cu–O bonds of Cu_2O which was exactly at the same position for both Cu_2O/CuO and Cu_2O/CuO/CuS-9. This is consistent with our previous reports.[38] However, modification of the Cu_2O/CuO surface with CuS causes shift in a broad intense peak located at 2.4 Å (black colored curve in Figure 7(b)), that matches well with Cu–Cu bonds, to the higher energy position implying the incorporation of the CuS. More interestingly, the Cu_2O/CuO/CuS-9 photoelectrode after PEC test has the same structural features with the Cu_2O/CuO/CuS-9 photoelectrode before PEC test, indicating better structural stability, however the intensity of the Cu–Cu bond in Cu_2O/CuO after the PEC test increases significantly compared to its initial state, indicating an

increase in the crystalline size of Cu_2O, probably due to the reduction of the CuO layer. The results displayed here are consistent with the XANES results.

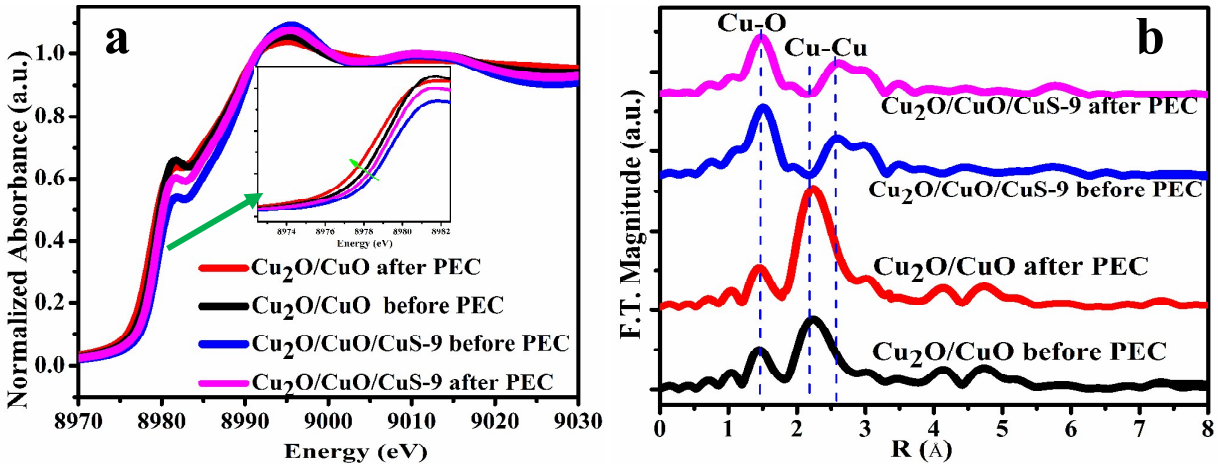

Figure 7. (a) Cu-K-edge XANES spectra of Cu_2O/CuO and Cu_2O/CuO/CuS-9 both before and after PEC; the inset showing enlargement in the region shown (b) Cu-K-edge EXAFS spectra of Cu_2O/CuO and Cu_2O/CuO/CuS-9 both before and after PEC in r space.

The elemental composition of Cu_2O/CuO and Cu_2O/CuO/CuS-9 were further investigated by XPS to examine the change in chemical status of Cu atom in the samples. Figure 8a shows the XPS survey spectrum of Cu_2O/CuO and Cu_2O/CuO/CuS-9. From the Cu_2O/CuO sample only peaks characteristics of Cu 2p, O 1s, and C 1s can be observed, however the Cu_2O/CuO/CuS-9 sample have additional signal that corresponds to S 2p. The weak peaks of C come from adventitious hydrocarbon from XPS instrument itself. The high-resolution XPS spectra of Cu and S in the 2p region for Cu_2O/CuO/CuS-9 are shown in Figure 8(b) and (c), respectively. The Cu 2p spectra before the PEC test for 1 hour (Figure 8b) shows the binding energies of Cu 2p3/2 and Cu 2p1/2 peaks at 932.7 and 952.8 eV, respectively, which are typical values for Cu^{2+} in CuS materials.[39, 40] Meanwhile, two satellite peaks at 943.2 and 963.6 eV are observed, indicating the paramagnetic chemical state of Cu^{2+}.[41] The symmetrical nature of the two Cu 2p XPS peaks and the binding energy peaks observed for S2p spectrums at 162.0 and 163.1 eV (Figure 8c) which are attributed to the S2p3/2 and S2p1/2 states, respectively, also confirms the formation of CuS.[42] However, after PEC test for 1 h, the two satellite peaks in the Cu 2p XPS

spectrum (indicated by circle in Figure 8(b) almost vanishes and the binding energies of Cu 2p3/2 and Cu 2p1/2 slightly shift to lower values (932.5 and 952.4 eV), indicating the presence of Cu^{1+}. From this result, it is more reasonable to assume that after PEC test for 1 h, some amount of Cu^{2+} in CuS is reduced to Cu_2S, and it further demonstrates the electron transfer from the surface of Cu_2O/CuO to CuS for the partial reduction of CuS to Cu_2S. This is consistent with our XAS results.

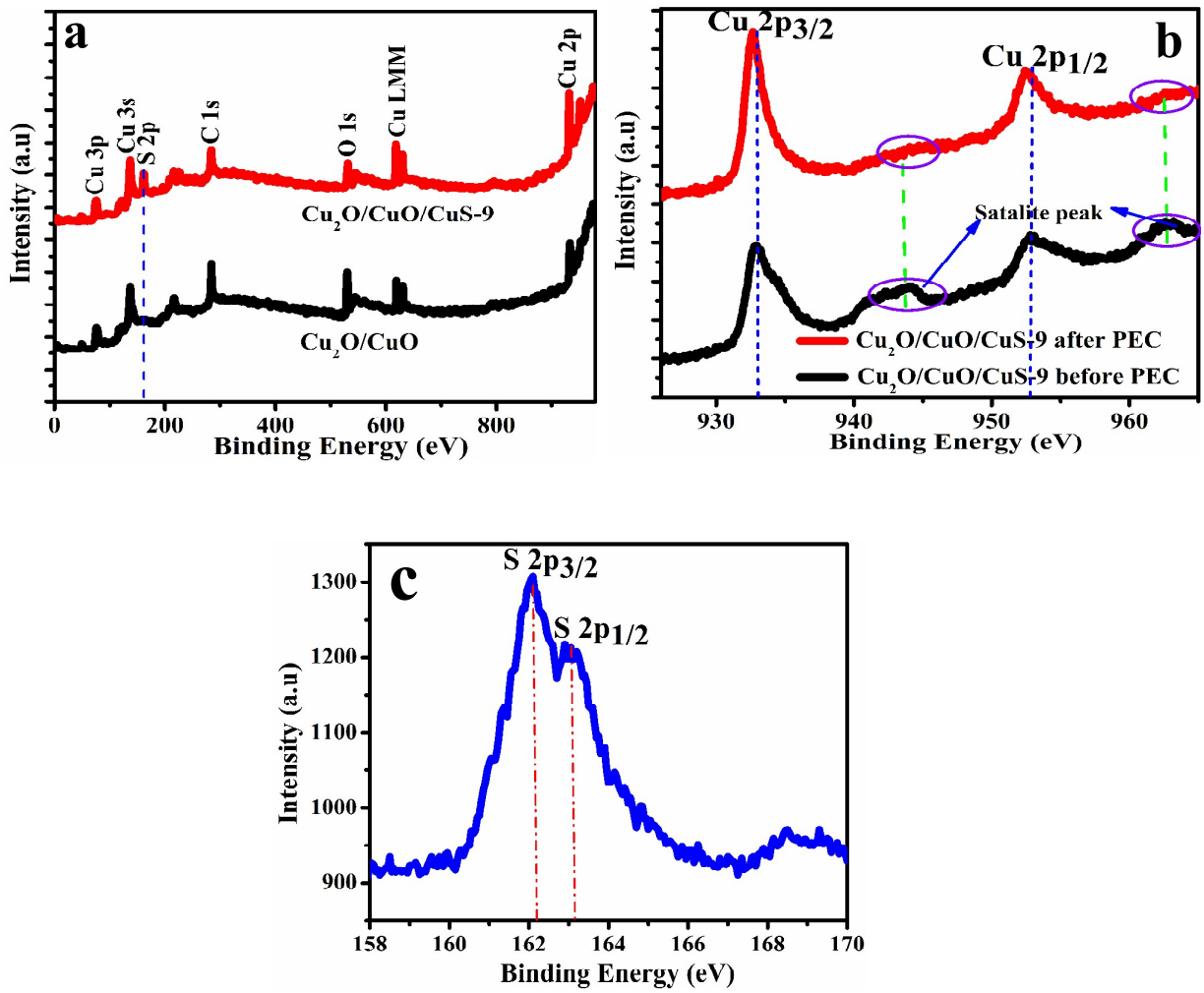

Figure 8. (a) Typical XPS survey spectra of Cu_2O/CuO and Cu_2O/CuO/CuS-9, and (b) Cu2p region of the XPS spectra of Cu_2O/CuO and Cu_2O/CuO/CuS-9 before and after 1 h PEC test (c) XPS S 2p spectrum of Cu_2O/CuO/CuS-9.

3.6 Proposed Charge Transfer Mechanism

Considering the band gaps (2.01 eV for Cu_2O and 1.54 eV for CuO) and the valence band values (0.63 V vs. RHE for Cu_2O and 0.74 V vs. RHE for CuO) reported in our previous study, the band energy level of Cu_2O/CuO/CuS in contact with electrolyte solution was illustrated in Scheme 2. Up on illumination of the photoelectrodes with visible light, it is clearly expected that band to band transition of photogenerated electrons would carried out as shown in Scheme 2 (green colored arrow). Because of the potential difference in the conduction or valence band of Cu_2O and CuO, the photogenerated electrons on conduction band of Cu_2O are transferred to the conduction band of CuO and the hole from CuO are transferred to the valence band of Cu_2O. However, we achieved a limited photocurrent density with the bare Cu_2O/CuO electrode, probably due to the sluggish kinetics in injecting photogenerated electron from the surface of the heterostructure to the electrolyte solution and due to self-reduction of the CuO layer by the accumulated electrons. More interestingly, introducing CuS on the surface of the Cu_2O/CuO heterostructure provided highly enhanced photocurrent density with appreciable stability. This is probably because the as deposited CuS causes fast transfer of accumulated photogenerated electrons from the Cu_2O/CuO surface (conduction band of CuO) to the aqueous solution for hydrogen production. Remarkably enhanced photocurrent density and stability is also suggested from the suppressed electron-hole recombination due to the interfacial charge transfer (IFCT) initiated by visible light illumination (indicated by dark red arrow in Scheme 2). The IFCT is theoretically proposed by Creutz et al. and in some other studies related to our work. [40, 43, 44] That is, the electrons in the valence band of CuO can be directly transferred to CuS under visible illuminations causing partial reduction of CuS to Cu_2S (already confirmed by XPS analysis) as shown in reaction 3 below, and the reduced Cu_2S state returns to CuS while generating H_2 according to reaction 4.

$$2CuS + 2e \longrightarrow Cu_2S + S^{2-} \quad (3)$$

$$Cu_2S + S^{2-} + 2H^+ \longrightarrow 2CuS + H_2 \quad (4)$$

Therefore, the CuS/Cu_2S cluster located at a potential of −0.5 V (vs SHE, pH = 0) acts as an electron sink and cocatalyst to promote the separation and transfer of photogenerated electrons from the surface of the Cu_2O/CuO to the CuS/Cu_2S cluster, where H^+ is reduced to hydrogen molecules.[40] Thus, the improved photocurrent density and high stability by Cu_2O/CuO/CuS heterostructure is because CuS not only promotes charge separation, but also reduces the bulk

and surface electron-hole recombination. It is very important to consider the optimum amount of CuS because, CuS deficiency increases electron-hole recombination while excess CuS blocks incident light and reduces the photocatalytic activity of the heterostructure. We believe that the synergistic effects induced by forming Cu_2O/CuO heterojunction and the incorporation of CuS cocatalyst greatly accelerate electron transfer and effectively retard the reduction of CuO by photo-generated electrons.

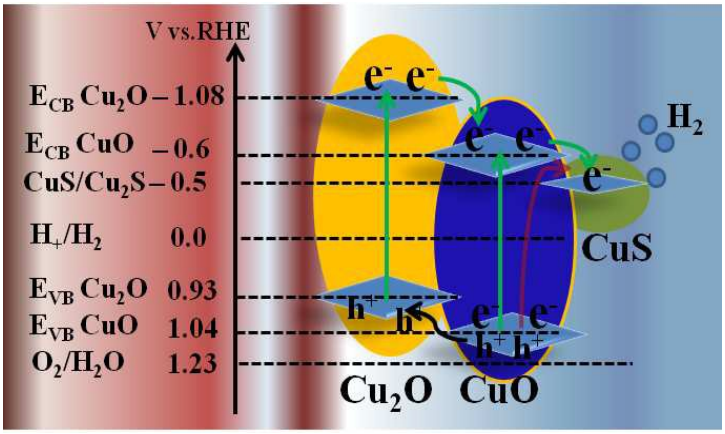

Scheme 2. Schematic illustration of band energy levels and charge transfers for the Cu_2O-CuO-CuS photocathode

Conclusions

To summarize, we have demonstrated a highly efficient and promising CuS modified Cu_2O/CuO heterostructure for water splitting hydrogen production using simple, low cost and scalable electrodeposition, thermal annealing and SILAR method. Both the photocurrent density and photostability are significantly enhanced by loading CuS as a cocatalyst over Cu_2O/CuO heterostructure. The optimal CuS SILAR deposition cycle is determined to be 9 (i.e. Cu_2O/CuO/CuS-9) and the photoelectrode reveals a 2.5 and 1.5 times increase in photocurrent density (–5.4 mA/cm^2) and photostability (85%) respectively, compared with the bare Cu_2O/CuO heterostructure. More importantly, the Cu_2O/CuO heterostructure modified with optimum CuS produces an impressive solar conversion efficiency of ABPE% = 3.6% which is greater than fourfold increase compared with the bare Cu_2O/CuO. It is believed that solar light illumination causes interfacial charge transfer from CuO to CuS, which results in the partial reduction of CuS

to Cu_2S and efficient band to band electron excitation and separation between Cu_2O and CuO due to their appropriate band alignment, and thus the separated and accumulated electrons in the conduction band of CuO flows to CuS/Cu_2S clusters. Since the potential of CuS/Cu_2S is about –0.5 V (vs SHE, pH = 0), which is more negative than H^+/H_2 potential, favors the reduction of H^+, thus enhancing the PEC performance of the photoelectrode. This study demonstrates a possibility for the use of low cost and abundant CuS as a substitute for noble metals as cocatalyst in the photocatalytic H_2 production.

Acknowledgments

The financial supports from the Ministry of Science and Technology (MoST)(103-3113-E-011 -001, 101-3113-E-011-002, 101-2923-E-011-001-MY3, 100-2221-E-011-105-MY3), and the Top University Projects of Ministry of Education (MOE) (100H451401), as well as the facilities supports from the National Synchrotron Radiation Research Center (NSRRC) and National Taiwan University of Science and Technology (NTUST) are acknowledged.

References

1. M. Moriya, T. Minegishi, H. Kumagai, M. Katayama, J. Kubota and K. Domen,Stable Hydrogen Evolution from CdS-Modified CuGaSe2 Photoelectrode under Visible-Light Irradiations *J. Am. Chem. Soc.*, 2013, **135**, 3733-3735.
2. A. A. Dubale, C.-J. Pan, A. G. Tamirat, H.-M. Chen, W.-n. Su, C.-H. Chen, J. F. Rick, D. W. Ayele, B. A. Aragaw, J.-F. Lee, Y.-W. Yang and B. J. Hwang,Heterostructured Cu2O/CuO decorated with nickel as a highly efficient photocathode for photoelectrochemical water reductions *J. Mater. Chem. A*, 2015, **3,**, 12482-12499.
3. W.-Y. Cheng, T.-H. Yu, K.-J. Chao and S.-Y. Lu,Cu2O-decorated CdS nanostructures for high efficiency visible light driven hydrogen productions *Int. J. Hydrogen Energy*, 2013, **38**, 9665-9672.
4. S. Xu, J. Ng, A. J. Du, J. Liu and D. D. Sun,Highly efficient TiO2 nanotube photocatalyst for simultaneous hydrogen production and copper removal from waters *Int. J. Hydrogen Energy*, 2011, **36**, 6538-6545.
5. S. K. Apte, S. N. Garaje, G. P. Mane, A. Vinu, S. D. Naik, D. P. Amalnerkar and B. B. Kale,A Facile Template-Free Approach for the Large-Scale Solid-Phase Synthesis of CdS Nanostructures and Their Excellent Photocatalytic Performances *Small*, 2011, **7**, 957-964.
6. K. Sivula, F. L. Formal and M. Grätzel,WO3−Fe2O3 Photoanodes for Water Splitting: A Host Scaffold, Guest Absorber Approachs *Chemistry of Materials*, 2009, **21**, 2862-2867.
7. S. Xu, A. J. Du, J. Liu, J. Ng and D. D. Sun,Highly efficient CuO incorporated TiO2 nanotube photocatalyst for hydrogen production from waters *Int. J. Hydrogen Energy*, 2011, **36**, 6560-6568.
8. M. Li, L. Zhao and L. Guo,Preparation and photoelectrochemical study of BiVO4 thin films deposited by ultrasonic spray pyrolysiss *Int. J. Hydrogen Energy*, 2010, **35**, 7127-7133.

9. X.-Y. Zhang, H.-P. Li, X.-L. Cui and Y. Lin,Graphene/TiO2 nanocomposites: synthesis, characterization and application in hydrogen evolution from water photocatalytic splittings *J. Mater. Chem.*, 2010, **20**, 2801-2806.
10. A. Paracchino, J. C. Brauer, J.-E. Moser, E. Thimsen and M. Graetzel,Synthesis and Characterization of High-Photoactivity Electrodeposited Cu2O Solar Absorber by Photoelectrochemistry and Ultrafast Spectroscopys *J. Phys. Chem. C*, 2012, **116**, 7341-7350.
11. A. Radi, D. Pradhan, Y. Sohn and K. T. Leung,Nanoscale Shape and Size Control of Cubic, Cuboctahedral, and Octahedral Cu−Cu2O Core−Shell Nanoparticles on Si(100) by One-Step, Templateless, Capping-Agent-Free Electrodepositions *ACS Nano*, 2010, **4**, 1553-1560.
12. A. Paracchino, V. Laporte, K. Sivula, M. GrÃ¤tzel and E. Thimsen,Highly active oxide photocathode for photoelectrochemical water reductions *Nat. Mater.*, 2011, **10**, 456-461.
13. Y.-F. Zhao, Z.-Y. Yang, Y.-X. Zhang, L. Jing, X. Guo, Z. Ke, P. Hu, G. Wang, Y.-M. Yan and K.-N. Sun,Cu2O Decorated with Cocatalyst MoS2 for Solar Hydrogen Production with Enhanced Efficiency under Visible Lights *J. Phys. Chem. C*, 2014, **118**, 14238-14245.
14. A. Paracchino, V. Laporte, K. Sivula, M. Grätzel and E. Thimsen,Highly active oxide photocathode for photoelectrochemical water reductions *Nat. Mater.*, 2011, **10**, 456-461.
15. C. Li, T. Hisatomi, O. Watanabe, M. Nakabayashi, N. Shibata, K. Domen and J.-J. Delaunay,Positive onset potential and stability of Cu2O-based photocathodes in water splitting by atomic layer deposition of a Ga2O3 buffer layers *Energy Environ. Sci*, 2015, **8**, 1493-1500.
16. A. Paracchino, N. Mathews, T. Hisatomi, M. Stefik, S. D. Tilley and M. Gratzel,Ultrathin films on copper(i) oxide water splitting photocathodes: a study on performance and stabilitys *Energy Environ. Sci*, 2012, **5**, 8673-8681.
17. Q. Huang, F. Kang, H. Liu, Q. Li and X. Xiao,Highly aligned Cu2O/CuO/TiO2 core/shell nanowire arrays as photocathodes for water photoelectrolysiss *J. Mater. Chem. A*, 2013, **1**, 2418-2425.
18. Z. Zhang and P. Wang,Highly stable copper oxide composite as an effective photocathode for water splitting via a facile electrochemical synthesis strategys *J. Mater. Chem.*, 2012, **22**, 2456-2464.
19. C.-Y. Lin, Y.-H. Lai, D. Mersch and E. Reisner,Cu2O|NiOx nanocomposite as an inexpensive photocathode in photoelectrochemical water splittings *Chem. Sci.*, 2012, **3**, 3482-3487.
20. P. Bornoz, F. F. Abdi, S. D. Tilley, B. Dam, R. van de Krol, M. Graetzel and K. Sivula,A Bismuth Vanadate–Cuprous Oxide Tandem Cell for Overall Solar Water Splittings *J. Phys. Chem. C*, 2014, **118**, 16959-16966.
21. S. D. Tilley, M. Schreier, J. Azevedo, M. Stefik and M. Graetzel,Ruthenium Oxide Hydrogen Evolution Catalysis on Composite Cuprous Oxide Water-Splitting Photocathodess *Adv. Funct. Mater.*, 2014, **24**, 303-311.
22. C. G. Morales-Guio, S. D. Tilley, H. Vrubel, M. Gratzel and X. Hu,Hydrogen evolution from a copper(I) oxide photocathode coated with an amorphous molybdenum sulphide catalysts *Nat. Commun.*, 2014, **5**.
23. C. G. Morales-Guio, L. Liardet, M. T. Mayer, S. D. Tilley, M. Grätzel and X. Hu,Photoelectrochemical Hydrogen Production in Alkaline Solutions Using Cu2O Coated with Earth-Abundant Hydrogen Evolution Catalystss *Angew. Chem. Int. Ed.*, 2015, **54**, 664-667.
24. K. Chang, Z. Mei, T. Wang, Q. Kang, S. Ouyang and J. Ye,MoS2/Graphene Cocatalyst for Efficient Photocatalytic H2 Evolution under Visible Light Irradiations *ACS Nano*, 2014, **8**, 7078-7087.
25. X. Zong, J. Han, G. Ma, H. Yan, G. Wu and C. Li,Photocatalytic H2 Evolution on CdS Loaded with WS2 as Cocatalyst under Visible Light Irradiations *J. Phys. Chem. C*, 2011, **115**, 12202-12208.
26. Y. Wang, X. Zhang, P. Chen, H. Liao and S. Cheng,In situ preparation of CuS cathode with unique stability and high rate performance for lithium ion batteriess *Electrochimica Acta*, 2012, **80**, 264-268.

27. L. Yi, Y. Liu, N. Yang, Z. Tang, H. Zhao, G. Ma, Z. Su and D. Wang,One dimensional CuInS2-ZnS heterostructured nanomaterials as low-cost and high-performance counter electrodes of dye-sensitized solar cellss *Energy Environ. Sci*, 2013, **6**, 835-840.
28. X. Meng, G. Tian, Y. Chen, R. Zhai, J. Zhou, Y. Shi, X. Cao, W. Zhou and H. Fu,Hierarchical CuS hollow nanospheres and their structure-enhanced visible light photocatalytic propertiess *CrystEngComm*, 2013, **15**, 5144-5149.
29. L. Yi, D. Wang and M. Gao,Synthesis of Cu3SnS4 nanocrystals and nanosheets by using Cu31S16 as seedss *CrystEngComm*, 2012, **14**, 401-404.
30. C. X. Shen S, Ren F, Kronawitter CX, Mao SS, Guo L.,Solar light-driven photocatalytic hydrogen evolution over ZnIn2S4 loaded with transition-metal sulfidess *Nanoscale Res. Lett*, 2011, **6**, 290.
31. L. Zhang, T. Jiang, S. Li, Y. Lu, L. Wang, X. Zhang, D. Wang and T. Xie,Enhancement of photocatalytic H2 evolution on Zn0.8Cd0.2S loaded with CuS as cocatalyst and its photogenerated charge transfer propertiess *Dalton Trans.*, 2013, **42**, 12998-13003.
32. Z.-Q. Y. Pu-Jun Jin, Mao-Lin Zhang, Yu-Hu Li and Hui-Ping Xing,A pigment (CuS) identified bymicro-Raman spectroscopy on a Chinese funerary lacquer ware of West Han Dynastys *J. Raman Spectrosc*, 2010, **41**, 222–225.
33. L A Isac, A Duta, A Kriza, I A Enesca and M. Nanu,The growth of CuS thin films by Spray Pyrolysiss *Journal of Physics: Conference Series* 2007, **61**, 477–481.
34. A. G. Tamirat, W.-N. Su, A. A. Dubale, H.-M. Chen and B.-J. Hwang,Photoelectrochemical water splitting at low applied potential using a NiOOH coated codoped (Sn, Zr) [small alpha]-Fe2O3 photoanodes *J. Mater. Chem. A*, 2015, **3**, 5949-5961.
35. X. Zhang, Y. Liu, S.-T. Lee, S. Yang and Z. Kang,Coupling surface plasmon resonance of gold nanoparticles with slow-photon-effect of TiO2 photonic crystals for synergistically enhanced photoelectrochemical water splittings *Energy Environ. Sci*, 2014, **7**, 1409-1419.
36. A. G. Tamirat, W.-N. Su, A. A. Dubale, C.-J. Pan, H.-M. Chen, D. W. Ayele, J.-F. Lee and B.-J. Hwang,Efficient photoelectrochemical water splitting using three dimensional urchin-like hematite nanostructure modified with reduced graphene oxides *J. Power Sources*, 2015, **287**, 119-128.
37. Z. Zhang, R. Dua, L. Zhang, H. Zhu, H. Zhang and P. Wang,Carbon-Layer-Protected Cuprous Oxide Nanowire Arrays for Efficient Water Reductions *ACS Nano*, 2013, **7**, 1709-1717.
38. A. A. Dubale, W.-N. Su, A. G. Tamirat, C.-J. Pan, B. A. Aragaw, H.-M. Chen, C.-H. Chen and B.-J. Hwang,The synergetic effect of graphene on Cu2O nanowire arrays as a highly efficient hydrogen evolution photocathode in water splittings *J. Mater. Chem. A*, 2014, **2**, 18383-18397.
39. E. Hong, D. Kim and J. H. Kim,Heterostructured metal sulfide (ZnS–CuS–CdS) photocatalyst for high electron utilization in hydrogen production from solar water splittings *Journal of Industrial and Engineering Chemistry*, 2014, **20**, 3869-3874.
40. J. Zhang, J. Yu, Y. Zhang, Q. Li and J. R. Gong,Visible Light Photocatalytic H2-Production Activity of CuS/ZnS Porous Nanosheets Based on Photoinduced Interfacial Charge Transfers *Nano Lett.*, 2011, **11**, 4774-4779.
41. J. Ghijsen, L. H. Tjeng, J. van Elp, H. Eskes, J. Westerink, G. A. Sawatzky and M. T. Czyzyk,Electronic structure of Cu2O and CuOs *Physical Review B*, 1988, **38**, 11322-11330.
42. Y. C. Zhang, T. Qiao and X. Ya Hu,A simple hydrothermal route to nanocrystalline CuSs *J. Cryst. Growth*, 2004, **268**, 64-70.
43. C. Creutz, B. S. Brunschwig and N. Sutin,Interfacial Charge-Transfer Absorption: 3. Application to Semiconductor−Molecule Assemblies†s *J. Phys. Chem. B*, 2006, **110**, 25181-25190.
44. M. Lee and K. Yong, Highly efficient visible light photocatalysis of novel CuS/ZnO heterostructure nanowire arrayss *Nanotechnology* 2012, **23,** , 194014.

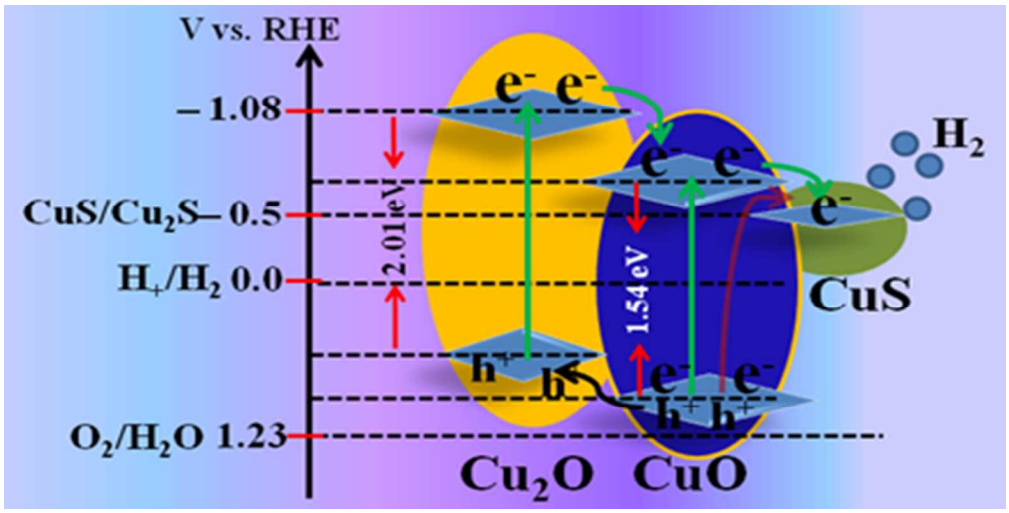

227x114mm (150 x 150 DPI)